Journal of Catalysis **202,** 118–128 (2001)
doi:10.1006/jcat.2001.3262, available online at http://www.idealibrary.com on IDEAL®

Titania-Supported Cobalt and Cobalt–Phosphorus Catalysts: Characterization and Performances in Ethane Oxidative Dehydrogenation

Younes Brik,*,† Mohamed Kacimi,* Mahfoud Ziyad,*,[1] and François Bozon-Verduraz†

*Faculté des Sciences, Département de Chimie, Laboratoire de Physico-chimie des Matériaux et Catalyse, Avenue Ibn Battouta, B.P. 1017, Rabat, Morocco; and †Laboratoire de Chimie des Matériaux Divisés et Catalyse, Université Paris 7-Denis Diderot, 2, place Jussieu, 75251 Paris cedex 05, France

Received January 25, 2001; accepted April 26, 2001

TiO_2-supported Cobalt and cobalt–phosphorus catalysts prepared by impregnation are characterized by XRD, XPS, Laser Raman Spectroscopy (LRS), and Diffuse Reflectance Spectroscopy (DRS) and investigated in ethane oxidative dehydrogenation (ODH). At low cobalt loadings, the carrier is essentially covered by octahedral Co^{2+} ions, whereas at concentrations superior to 3.7 wt% formation of the Co_3O_4 spinel is observed. The best performance in ethane ODH is achieved at 550°C with the sample containing 7.6 wt% Co. The reaction begins with a conversion of 33% and a selectivity around 75%, then it decreases to reach after 150 min on stream a stationary state at 22% of conversion and 60% selectivity. This loss of 30% of the initial activity may be associated with a decrease of the specific surface area and the concomitant formation of $CoTiO_3$ and Co_2TiO_4, as revealed by LRS, *in situ* DRS, and XPS analysis. The activity in ethane ODH seems to be mainly related to the presence of Co^{2+} ions octahedral sites. Addition of phosphorus to Co(7.6)/TiO_2 catalysts results in the reduction of Co^{3+} ions and a growth of amorphous cobalt–phosphorus compounds which provoke a severe decrease of the catalyst performance.

Key Words: **ethane oxidative dehydrogenation; cobalt–TiO_2 catalysts; phosphorus–cobalt–TiO_2 catalysts; *in situ* diffuse reflectance spectroscopy; laser Raman spectroscopy; XPS.**

1. INTRODUCTION

The catalytic partial oxidation of light alkanes into alkenes and oxygenated products has been widely investigated in the recent years for commercial and academic goals. It offers an alternative to the pyrolysis processes presently used and promises to provide cheaper production of chemicals from the available raw materials. Vanadium, molybdenum, and niobium oxides are often present in the catalysts (1). Thorsteinson *et al.* have reported that the system Mo–V–Nb–O leads in ethane ODH to an ethylene selectivity of 100% at 10% conversion (2). Better performances have been claimed by Murakami *et al.* using boron oxides on different carriers. On 30 wt% B_2O_3 loaded alumina, the ethylene yield was equal to 14.6% at 38% conversion (3). It has been also reported that the system made of Co, Zr, P, Fe, and K oxides can give a selectivity of 74% at 53% conversion (4). Comparing several chromium loaded lamellar phosphates, Loukah *et al.* showed that $CrPO_4$ exhibits an ethylene selectivity of 60% at 30% conversion (5). On vanadium phosphates (VOP) investigated in analogous conditions, the selectivity reaches 70% at 20% conversion. On V/TiO_2 modified by phosphorus, El-Idrissi *et al.* (6) reported an ethylene selectivity of 50% at 33% conversion for a P/V ratio of 1.64. The authors concluded that the performances are governed by acid–base properties and the V^{4+}/V^{5+} ratio. They attributed the gain in selectivity to the ability of phosphorus to adjust the surface acidity and increase the amount of isolated V^{4+} species. These vanadium based catalysts still initiate investigations and several papers have been lately published on their ODH abilities (7).

Cobalt supported catalysts are known to be efficient in hydrotreatment, Fischer–Tropsch reactions, and related syntheses (8). When titania is the support, decoration effects decrease the activity in benzene and CO hydrogenation (9). Cobalt catalysts were also studied in the coupling of methane (10). Incorporated in perovskite-type materials like $LnCoO_3$, cobalt exhibits a good activity in total oxidation and in pollution control reactions (11). Most of the authors attribute the catalytic activity of perovskites to their nonstoichiometric properties and their propensity to release oxygen (12). As a matter of fact, Co^{2+} ions being quite difficult to oxidize, the typical Mars and Van Krevelen redox mechanism cannot easily be applied to ODH reactions. Therefore, whenever oxygen is part of the oxidation process, the oxidative properties of cobalt can be accredited to oxygen species that appear on the surface of the catalyst (13).

[1] To whom correspondence should be addressed. E-mail: ziyad@fsr.ac.ma.

0021-9517/01 $35.00

The present work is devoted to the study of ethane oxidative dehydrogenation (ODH) over different cobalt and cobalt–phosphorus loaded TiO_2. This system to our knowledge has not yet been investigated in light alkanes ODH. Moreover, the interactions between cobalt and titania, previously examined in reducing conditions (9), deserve particular consideration in atmospheres containing a reducing as well as an oxidizing agent (14). Special attention is also paid to the characterization of the solids before and after the catalytic tests using XRD, XPS, Laser Raman, and *in situ* Diffuse Reflectance Spectroscopy. Attempts are made to correlate the ODH results with the catalysts' composition and the nature of the active sites.

2. EXPERIMENTAL

2.1. Preparation of Catalysts and Model Compounds

The TiO_2 sample used as a carrier has the anatase structure and a specific surface of 89 $m^2\ g^{-1}$. It was purchased from Rhône-Poulenc (TiO_2 DT51) and was used without any further treatment. Chemical analysis revealed that it contains less than 4% of sulphates. Several samples loaded with various amounts of cobalt and labeled Co(x)/TiO_2 (with $x = 0.7$, 1.8, 3.7, 7.6, 11.5, and 15.6 wt% Co) were prepared by impregnation of the support by an excess of a $Co(NO_3)_2$, $6H_2O$ solution of adequate concentration (pH 5.2). The suspension was maintained under stirring at 80°C until complete evaporation of water. The recovered solids were dried at 120°C and calcined at 550°C for 4 h under flowing air (30 $cm^3\ min^{-1}$) in a rotating reactor. Phosphorus addition to Co(7.6)/TiO_2 was performed using the same procedure and solutions containing different concentrations of $(NH_4)_2HPO_4$. Four compositions labeled P(y)Co(7.6)/TiO_2 were prepared taking $y = 2.1$, 4.3, 6.5, and 8.6 wt% P.

The specific surface area of the samples evacuated for 2 h at 300°C was measured, before and after the catalytic tests, by nitrogen adsorption at −196°C with a Micromeritics apparatus. It appears that the specific surface area decreases when the cobalt content increases and after performing the catalytic reaction but increases slightly upon introduction of phosphorus (Table 1). Co_3O_4 was synthesized by calcination of $Co(NO_3)_2$, $6H_2O$ at 550°C in air. Pure Co_2TiO_4 and $CoTiO_3$ were obtained by heating TiO_2 impregnated with stoichiometric quantity of cobalt(II) nitrate at 1150°C in air for 4 h.

2.2. Characterization Techniques

X-ray diffraction patterns were recorded on a Siemens D500 high resolution spectrometer using Cu $K\alpha$ radiation ($\lambda_K\alpha = 1.540598$). The data were collected with a step of 0.02° (2θ) at room temperature. The crystallite size of Co_3O_4 was estimated from the (311) line using the Scherrer equation and a counting time of 30 s per step (2θ) of 0.005°.

Laser Raman (LR) spectra were obtained in backscattering geometry with a Dilor XY spectrometer using the 514.5 nm excitation line of a coherent argon Spectra Physics Laser model 165. The data were collected keeping the power under 20 mw. The spectrometer was also equipped with a monochromator used in the subtractive mode to select a given spectral range and a Jobin–Yvon 1024* 256 CCD matrix cooled thermoelectrically as the multichannel detector.

Diffuse Reflectance (DR) spectra were recorded between 190 and 2500 nm, using 300 mg of the sample, on a Varian Cary 5E spectrometer equipped with an integrating sphere coated with polytetrafluoroethylene (PTFE). For *in situ* examination, in reaction conditions, a special optical accessory (Praying Mantis from Harrick) was employed (15, 16). It is equipped with a stainless-steel chamber allowing one to work under controlled atmosphere and temperatures up to 550°C. To avoid problems related with light emission by the samples, the spectra were recorded after cooling to room temperature. In all cases PTFE was used as the reference.

XPS spectra were recorded on a Vacuum Generators MK I spectrometer with an unmonochromated Al $K\alpha$ (1486.6 eV, 200 watts) under about 10^{-9} Torr. The spectra were digitized, summed, smoothed, and reconstructed using Gauss–Lorentzian components. The measurements were carried out on powdered samples dispersed on an indium plaque, using the C1s peak at 285 eV as a referrence. The surface composition of the samples was estimated from XPS peak areas and corrected by the difference in cross sections according to Scofield data (17).

2.3. Catalytic Tests

The ethane ODH was carried out in a quartz U-shaped continuous flow microreactor operating at atmospheric pressure. Prior to the reaction, the catalyst (100 mg) was sieved to a grain size ranging from 125 to 180 μm, put into the reactor between two quartz wool plugs then flashed

TABLE 1

Specific Surface Areas (m^2/g) of P(y)Co(x)/TiO_2 before and after the Catalytic Tests

Samples	TiO_2	$x = 0.7$	$x = 1.8$	$x = 3.7$	$x = 7.6$	$x = 11.5$	$x = 15.6$	$y = 2.1$	$y = 4.3$	$y = 6.5$	$y = 8.6$
Before tests	89	81.6	71.2	68.2	63.5	61.3	60.8	68.1	67.5	66.2	67.6
After tests	81.2	54	50.2	47.6	40.7	38.4	37.6	47	46.2	53	52

with a stream of pure nitrogen. The reaction mixture was composed of 6 vol.% of ethane, 3 vol.% of O_2 and 91 vol.% of N_2. Analysis of the effluent gases was performed on two on-line chromatographs, a FID equipped with a Porapak Q column (for hydrocarbons), and a catharometer with a silica gel column (for oxygenated products). Under the selected experimental conditions the reaction starts around 300°C and produces only ethylene and CO_x.

3. RESULTS AND DISCUSSION

3.1. Catalysts Characterization before the Catalytic Tests

XRD patterns. For cobalt loadings ranging from 0.7 to 3.7 wt%, the Co(x)/TiO_2 diagrams (Fig. 1) exhibit only the anatase characteristic peaks (JCPDS file number 84-1286). Above 3.7 wt% Co, besides anatase, peaks ascribed to the Co_3O_4 spinel are detected (JCPDS file number 78-1970). Their intensity increases with the cobalt concentration. The particle size also increases slightly from 17 to 19 nm when the Co content increases from 5.6 to 15.6% in agreement with the data published by Ho *et al.* (9). These authors were able to detect Co_3O_4 crystallites at Co loadings as low as 1.5 wt% on a mixture of anatase and rutile (with a specific surface area of 50 $m^2\ g^{-1}$). This difference with our results may be ascribed to the larger surface area of our carrier (anatase), which allows a better dispersion of Co_3O_4 and probably even the formation of amorphous phases undetectable by XRD.

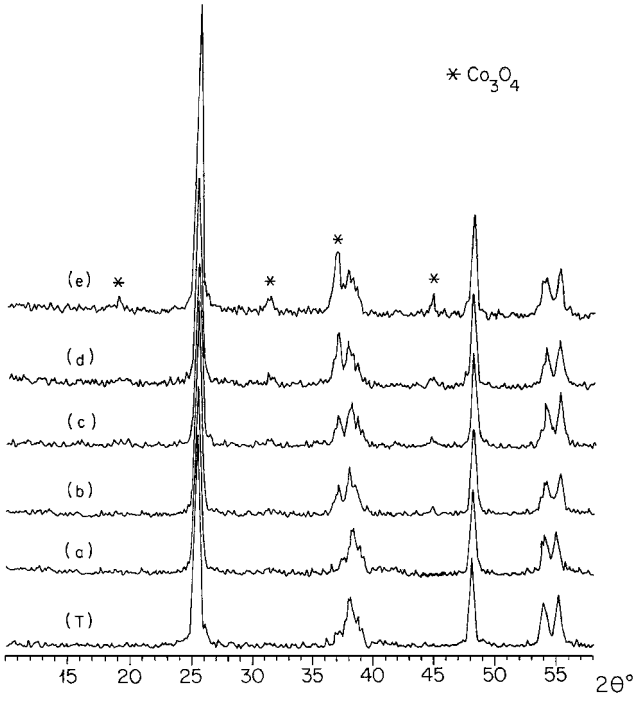

FIG. 1. XRD patterns of (T) TiO_2, (a) Co(3.7), (b) Co(5.6), (c) Co(7.6), (d) Co(11.5), and (e) Co(15.6).

Conversely, the XRD patterns of the phosphorus-loaded samples, P(y)Co(7.6)/TiO_2, (not presented), show that phosphorus prevents the growth of crystallized cobalt compounds, possibly through the formation of amorphous undetectable cobalt phosphates (18).

UV-visible NIR DRS. Previous studies have concerned cobalt catalysts supported on a variety of oxides and cobalt mixed oxides but, to our knowledge, none was devoted to the cobalt–titania system. The band positions and assignments concerning this system are presented in Table 2 including the data obtained on reference compounds and related systems (19–27). As preliminary remarks, it must be underlined that the distinction between the different Co^{n+} entities is not straightforward for two reasons: (i) in the 1100–1500 nm range, the ν_1 transition of the octahedral Co^{2+} ions overlaps, at least partially, the ν_2 transition of the tetrahedral species. Moreover, the higher absorption coefficient of the latter makes difficult the detection of the former; (ii) on titania, $Co^{2+} \rightarrow Ti^{4+}$ intervalence charge transfer may occur. In Co^{2+}-doped $MgTi_2O_5$, an absorption in the 400–500 nm region has been ascribed to this type of transition (28). It should be stressed that this kind of transition must be considered every time the cations of both the support and the active phase have a variable valence.

The spectra of the carrier and of Co(x)/TiO_2 catalysts are presented in Fig. 2. In the UV range, the spectrum of TiO_2 displays a strong absorption due to the interband transition (valence band → conduction band). The maxima near 320 and 220 nm may be attributed to the $O^{2-} \rightarrow Ti^{4+}$ charge transfers. In the visible region, the Co(3.7)/TiO_2 sample (spectrum a) shows only a slight absorption adjacent to the titania absorption edge (400–500 nm), but for Co contents superior to 5.6 wt% new bands which intensify with Co loading appear:

- in the NIR region there is a broad band between 1200 and 1600 nm and the 2ν(OH) harmonics band of residual hydroxyl groups (near 1380 nm);
- in the visible domain there is another band centered near 700 nm and a shoulder between 400 and 600 nm, with a maximum at 420 nm detected only for the sample containing 15 wt% Co (spectrum e).

These results show that different cobalt species are present (cf. Table 2):

- at low Co content (3.7 wt%), octahedral Co^{2+} species characterized by weak bands ascribed to ν_1 in the NIR and ($\nu_2 + \nu_3$) in the visible domain are observed. The model system, for comparison purposes is the Co^{2+} ions in a MgO matrix (25). Moreover, in the 400–500 nm interval, contribution of $Co^{2+} \rightarrow Ti^{4+}$ intervalence charge transfer may be involved (28);
- for Co loadings superior to 5.6 wt% (spectra b to e), several bands appear: (i) in the visible range, a broad band

TABLE 2

UV–Visible-NIR Bands Positions (in nm) and Assignments of Cobalt Ions in Co(x)/TiO_2 Catalysts, Related Systems, and Reference Compounds

samples	Co^{2+} (Td)		Co^{2+} (Oh)			Co^{3+} (Oh)	
	ν_1 $^4A_2 \rightarrow {}^4T_1(F)$	ν_2 $^4A_2 \rightarrow {}^4T_1(P)$	ν_1 $^4T_{1g} \rightarrow {}^4T_{2g}(F)$	ν_2 $^4T_{1g} \rightarrow {}^4A_{2g}(F)$	ν_3 $^4T_{1g} \rightarrow {}^4T_{1g}(P)$	ν_1 $^1A_{1g} \rightarrow {}^1T_{1g}$	ν_2 $^1A_{1g} \rightarrow {}^1T_{2g}$
Co/TiO_2 This work	1530, 1350, 1250	**vw**. 630, 590	Masked by ν_1 of Td Co^{2+}	**sh** 760	**sh**. 500	700	420
$CoTiO_3$ This work	Contain only Co^{2+} in octahedral symmetry		1530	760	600	Contain only Co^{2+} in octahedral symmetry	
Co_2TiO_4 This work	1820-1300	670, 623, 580	**sh**. 1150	**sh** . 720	**sh** . 535	Contains 50% Co^{2+} in Oh symmetry and 50% Co^{2+} in Td Symmetry	
Co_3O_4 This work	1510, 1300, 1210	**w**. 630	Contains only Co^{2+} in tetrahedral symmetry			720	430
Co/Nb_2O_5 (19)	Spectra recorded between 200-1000nm	Not observed	masked because the extinction coefficients of tetrahedral Co^{2+} ions are much stronger than those of octahedral ions.			740	450
Co/Al_2O_3 (20)	Spectra recorded between 200-1000nm	Not observed				642	435
Co/Al_2O_3 (21)	1250, 1350, 1560	625, 590, 550				700	450
Co/SiO_2 (22)	Not observed	580, 650				710	410
$ZnCo_2O_4$ (23)	Contains only Co^{3+} in octahedral symmetry.					625	394
Co/ZnO (24)	1612, 1470, 1315	650, 600, 566	Contain only Co^{2+} in tetrahedral symmetry				
$Co/AlPO_4$ This work	1457, 1283	620, 582, 532					
$CoAl_2O_4$ (21)	1370	662, 588, 552					
Co/MgO (25)	Contain only Co^{2+} in octahedral symmetry		1176	581	526	Contain only Co^{2+} in octahedral symmetry	
CoNaY (26)			1250	725	Not observed		
CoO This work			1280	**sh.** (606, 770)	550		
Co_2SiO_4 (27)			Spectra recorded between 200-1000nm	775	556		
Co^{2+} in glasses (23)	1754, 1492, 1258	641, 592, 530	Contain only Co^{2+} in tetrahedral symmetry				
	1800, 1500, 1300	660, 610, 540					
	Not observed	645, 590, 530					

The ν_1 $^4A_2 \rightarrow {}^4T_2(F)$ transition of Co^{2+} (Td) appears in the IR region.
The ν_1' $^1A_{1g} \rightarrow {}^3T_{1g}$, $^3T_{2g}$ of octahedral Co^{3+} is spin forbidden.

centered near 700 nm, a shoulder in the 550–400 nm interval and for Co-richer sample (spectrum: e) maxima at 420, 590, and 630 nm (ii) in the NIR, a triplet with maxima around 1250, 1350, 1530 nm. Most of these bands indicate the formation of tetrahedral Co^{2+} species as illustrated by: ν_3 at 630 and 590 nm, ν_1 near 1250, 1350, 1530 nm, and the splitting arising from the degeneracy lift of the $^4T_1(F)$ and $^4T_1(P)$ excited levels by spin–orbit coupling and/or dynamic Jahn–Teller effect (26, 29). Moreover, octahedral Co^{3+} species are also present, as shown by the band centered at 700 nm and the shoulder around 420 nm (resolved only for 15 wt% Co), ascribed to the $^1A_{1g} \rightarrow {}^1T_{2g}(\nu_1)$ and $^1A_{1g} \rightarrow {}^1T_{1g}(\nu_2)$ transitions of low spin Co^{3+} ions in octahedral symmetry (29). This is consistent with the formation of the Co_3O_4 spinel

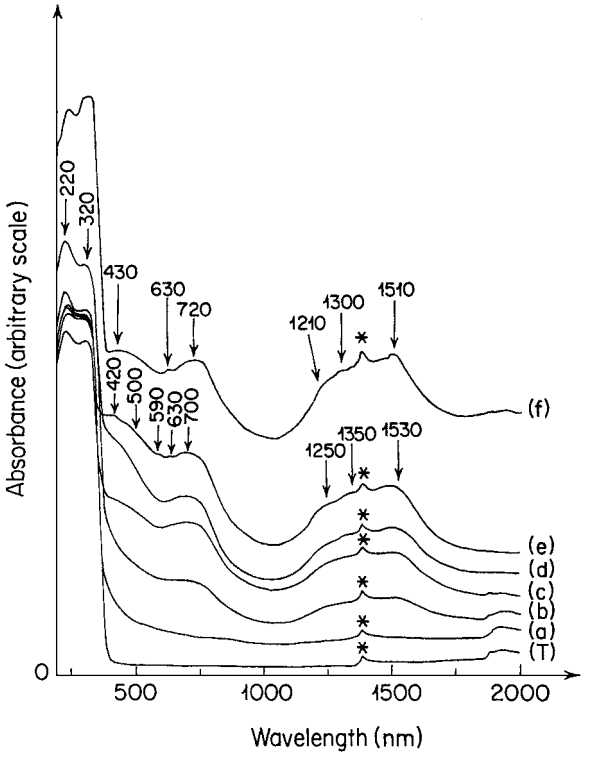

FIG. 2. DR Spectra of (T) TiO_2, (a) Co(3.7), (b) Co(5.6), (c) Co(7.6), (d) Co(11.5), (e) Co(15.6), (f) mechanical mixture of Co_3O_4 (10% wt) in titania. ($^*2\nu_{OH}$ harmonic band).

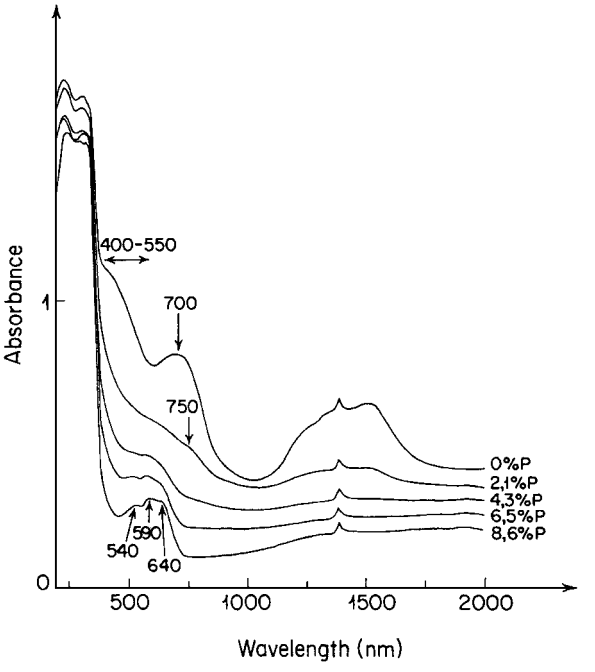

FIG. 3. Influence of phosphorus content on the DRS spectra of the Co(7.6))/TiO_2 sample.

which contains two octahedral Co^{3+} ions for one tetrahedral Co^{2+}. There is, indeed, a striking similarity between the spectrum of Co_3O_4 and the spectra of cobalt-rich catalysts (Fig. 2).

Diffuse reflectance spectra of the phosphorus-modified samples, P(y)Co(7.6)/TiO_2, are shown in Fig. 3. The ν_1 and ν_2 transitions assigned to octahedral Co^{3+} ions disappeared, whereas three new bands ascribed to the ν_3 transition of Co^{2+} ions in tetrahedral coordination are detected at 540, 590, and 630 nm. On the sample containing 2.1 wt% P, octahedral Co^{2+} species are still present as indicated by the ν_2 transition near 750 nm. However, there is also a marked decrease of the absorbance of all cobalt species. This attenuation might be due to the formation of new cobalt-containing species which modify, as suggested by XPS experiments (see below), the local structure and the environment of the cobalt sites. It remains that phosphorus addition reduces Co^{3+} ions and stabilizes divalent cobalt in tetrahedral symmetry (30). This tendency is reinforced when the amount of phosphorus in the samples is increased.

Laser Raman spectroscopy. In recent years, LRS has become an increasingly valuable tool for the investigation of supported and unsupported catalysts. The results obtained with Co(x)/TiO_2 are reported in Fig. 4. Anatase is characterized by three bands at 397, 514, and 640 cm^{-1} (Fig. 4, diagram T) and the spectrum does not seem to be affected by cobalt addition up to 3.7 wt% Co (diagram a), in agreement with the XRD and DRS results. For higher loadings ($\geq$5.6%), a band centered at 692 cm^{-1} and two shoulders at 487 and 528 cm^{-1} are observed, which confirms the

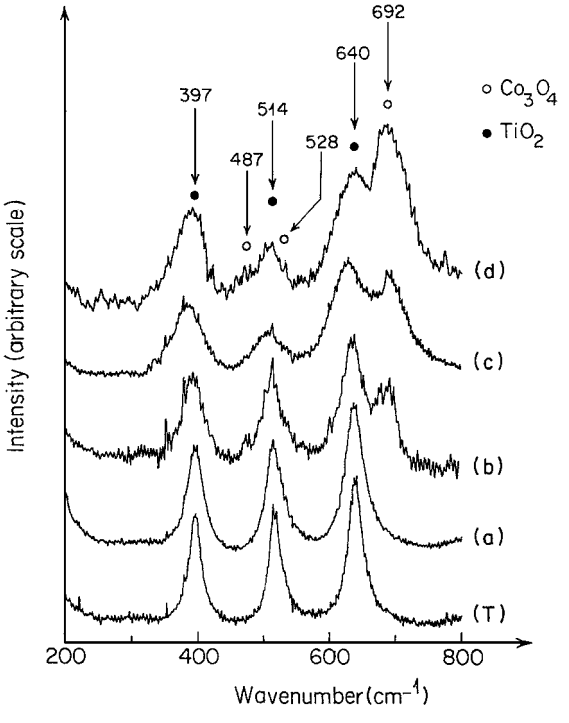

FIG. 4. Raman spectra of (T) TiO_2 and of Co(x)/TiO_2 catalysts (a) Co(3.7), (b) Co(5.6), (c) Co(7.6), and (d) Co(11.5).

formation of Co_3O_4 (31, 32). In contrast, phosphorus introduction in Co(7.6)/TiO_2 removes all Co_3O_4 peaks (figure not shown). Phosphorus contents superior to 6.5 wt% modify slightly the intensity of the bands due to the effect of undetectable amorphous cobalt species evoked above.

X-ray photoelectron spectra (XPS). The core levels of transition elements present generally a main peak (M) accompanied by an adjacent satellite (S) located at higher binding energy (BE). The complicated processes involved (shake-up peaks) are often interpreted in terms of ligands → metal charge transfers (33). The recent model of Veal (34), based on atomic relaxation, allows us to explain the multiplicity of the peaks subsequent to photoemission. In fact, in most cases, the spectral features allow the identification of the elements, the determination of their valence state, and the concentration on a surface. Quantitative data can be withdrawn from peak heights or peak areas. The identification of chemical states is often derived from measurement of peak positions and separations. Coordination geometry of the analyzed elements can be investigated by determining the intensity ratios of the satellite peak to the corresponding principal peak (S/M). ΔE is the shift in binding energy for a given core level of an atom in two distinct environments. Usually, there are significant changes in ΔE when the oxidation state of the metal is changed. In general, binding energies decrease with decreasing oxidation state.

The Co $2p_{3/2}$ core level spectra, the binding energies (BE), the S/M ratio (satellite intensity/main peak intensity), and the spin–orbit coupling ΔE (Co $2p_{1/2}$ − Co $2p_{3/2}$) are reported in Table 3. For the Co(x)/TiO_2 samples, when the cobalt loading increases, the Co $2p_{3/2}$ BE decreases from 781.2 to 779.9 eV and ΔE decreases from 15.8 to 15.1 eV. The results reported in Table 3 show, in agreement with the literature, an opposite behavior (35). This is because for many cobalt compounds, the conventional model based on ionic considerations does not fit the experimental data. Appropriate interpretations of the XPS results in the case of cobalt should take into account the effective charge distributed around the element in the solid (36).

To discuss the experimental results it is essential to point out that in the anatase structure, the plane (001) is the preferentially exposed and it exhibits octahedral vacant sites.

- At low cobalt loadings (0.7 up to 3.7 wt%) the Co^{2+} ions are incorporated into these sites with O^{2-} ions sitting on the top for charge compensation. The BE, S/M, and ΔE (Table 3) come closer to those of CoO as the cobalt concentration increases and are consistent with the predominance on the surface of Co^{2+} ions in octahedral symmetry.
- At high loadings, the amount of cobalt exceeds the TiO_2 dispersion capacity. All the vacant sites are occupied by highly dispersed CoO, and crystalline Co_3O_4 starts to appear. The BE, S/M, and ΔE decrease and become close to those of the Co_3O_4 spinel (37). This means that Co_3O_4 particles have been formed. These data are in accordance with the results previously reported by Ho *et al.* (9).

On the other hand, upon addition of phosphorus to Co(7.6)/TiO_2, the Co/Ti increases markedly suggesting that on the plane (001) of TiO_2 the Ti^{4+} sites are partially covered by phosphorus forming probably amorphous species. The ratio S/M increases to reach the value recorded at low cobalt loading probably because the Co^{3+} ions are reduced into Co^{2+}, which exhibit an intense satellite peak. Additional introduction of phosphorus increases its dispersion on the surface of the carrier.

3.2. Ethane ODH

The preliminary experiments carried out at 550°C showed that the conversion on pure TiO_2 does not exceed 5%. On Co(x)/TiO_2 catalysts at stationary state (Fig. 5), the ethane conversion and ethylene yield increase with the

TABLE 3

XPS Characterization of the Co/TiO_2 Samples and Reference Compounds

Samples	Co $2p_{3/2}$ BE	Co $2p_{3/2}$ S/M	ΔE	Co/Ti XPS	Co/Ti global	P/Co XPS	P/Co global
Co(0.7)/TiO_2	781.2	0.48	15.8	2.3×10^{-2}	1.01×10^{-2}	—	—
Co(1.8)/TiO_2	781.1	0.43	15.6	3.7×10^{-2}	2.56×10^{-2}	—	—
Co(3.7)/TiO_2	781	0.42	15.4	8.9×10^{-2}	5.26×10^{-2}	—	—
Co(7.6)/TiO_2	780.2	0.27	15.2	16×10^{-2}	11.11×10^{-2}	—	—
Co(15.6)/TiO_2	779.9	0.19	15.1	28.8×10^{-2}	25×10^{-2}	—	—
P(2.1)Co(7.6)/TiO_2	781.5	0.50	15.6	25.9×10^{-2}	11.11×10^{-2}	0.62	0.5
P(8.6)Co(7.6)/TiO_2	781.8	0.52	15.8	18.6×10^{-2}	11.11×10^{-2}	3.84	2
Co_2TiO_4	781	0.40	15.8	1.97	2	—	—
$CoTiO_3$	781.2	0.47	15.9	1	1	—	—
Co_3O_4	779.8	0.13	15.1	—	—	—	—
CoO	780.4	0.4	16	—	—	—	—

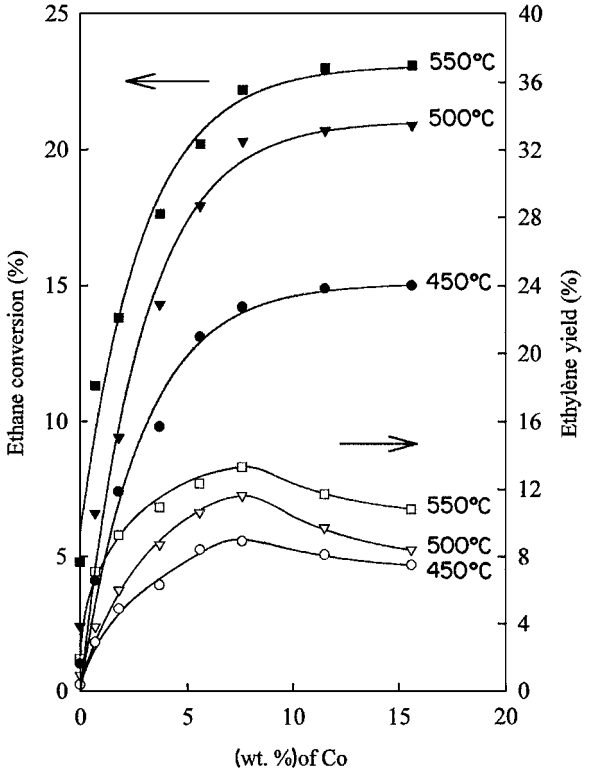

FIG. 5. Variation of ethane conversion (full) and ethylene yield (open) versus cobalt loading (wt%) at 450, 500, and 550°C.

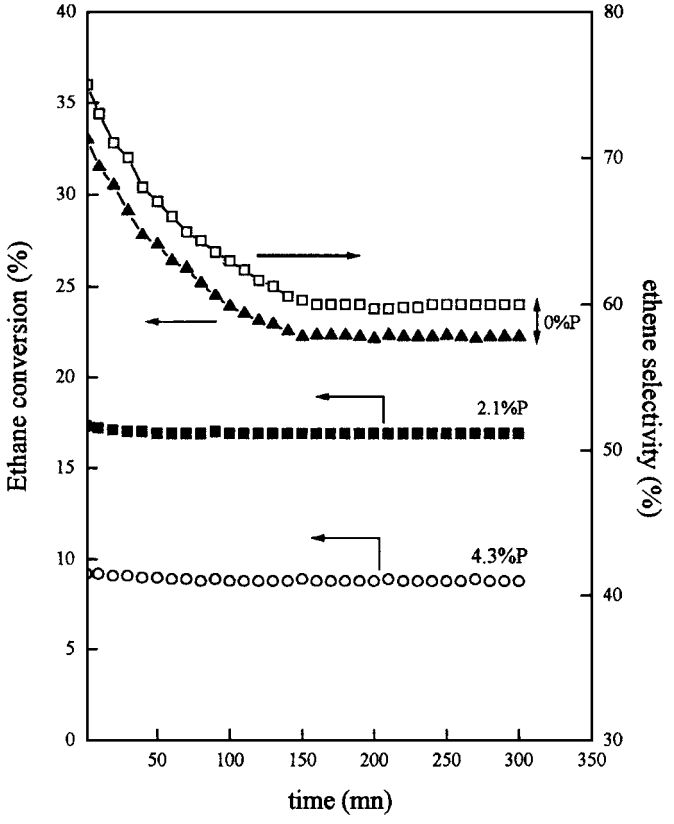

FIG. 6. $Co(7.6)/TiO_2$ sample: variation of the catalytic activity and ethylene selectivity in ethane ODH versus time at 550°C; influence of the phosphorus content on the activity.

reaction temperature in the 450–550°C interval. When the cobalt loading increases, the conversion increases sharply before attaining a plateau, whereas the ethylene yield passes through a maximum near 7.6 wt% Co. At 550°C the conversion obtained on $Co(7.6)/TiO_2$ reaches 22.2% with an ethylene yield of 13.3% (at 60% selectivity). Figure 6 represents the variation of ethane conversion versus time over $Co(7.6)/TiO_2$ at 550°C. The conversion decreases from 33% to around 22.2% at the stationary state, which is reached after 3 h of reaction. In the meantime, the specific surface area suffers a significant decrease and the catalyst color changes from light gray to green, probably because the coordination and/or the oxidation state of the cobalt cations changes also. For the comparison of the catalyst performances it is necessary to determine their selectivity at the same conversion under identical experimental conditions. The results obtained at 550°C are displayed in Fig. 7. It confirms that the best catalyst is $Co(7.6)/TiO_2$. Moreover, it shows that at low conversion the activation energy of the reaction is around 70 kJ mol^{-1} and is not dominated by the homogeneous processes.

In order to trace the catalyst's structural modifications throughout the catalytic tests, *in situ* DRS experiments were performed using 45 mg of the catalyst. The spectra recorded versus time on $Co(7.6)/TiO_2$ are displayed in Fig. 8. Before admitting the reaction mixture in the reactor ($t = 0$), the sample was heated up to 550°C in flowing nitrogen, which explains the disappearance of the $2\nu(OH)$ harmonics near 1380 nm. Introduction of the reaction mixture at 550°C leads to spectral changes which are enhanced with time on

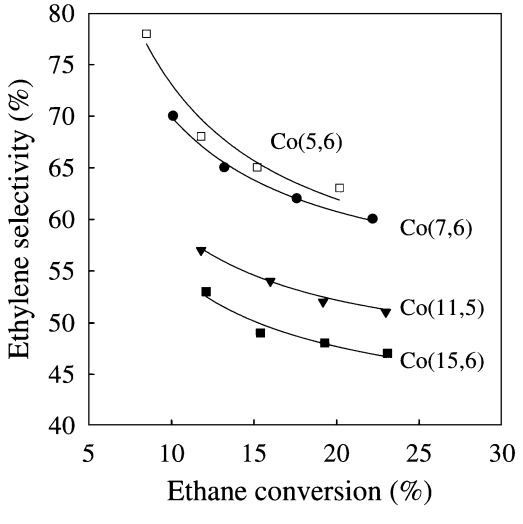

FIG. 7. Variation of ethylene selectivity versus ethane conversion at 550°C and different cobalt loadings.

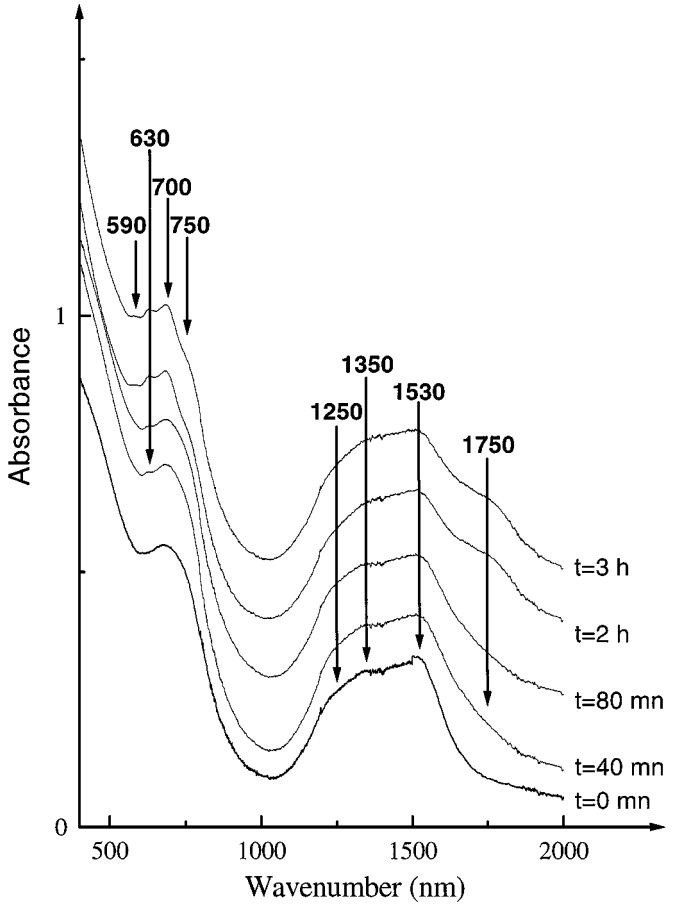

FIG. 8. *In situ* DRS of the Co(7.6)/TiO_2 catalyst versus time during ODH of ethane at 550°C.

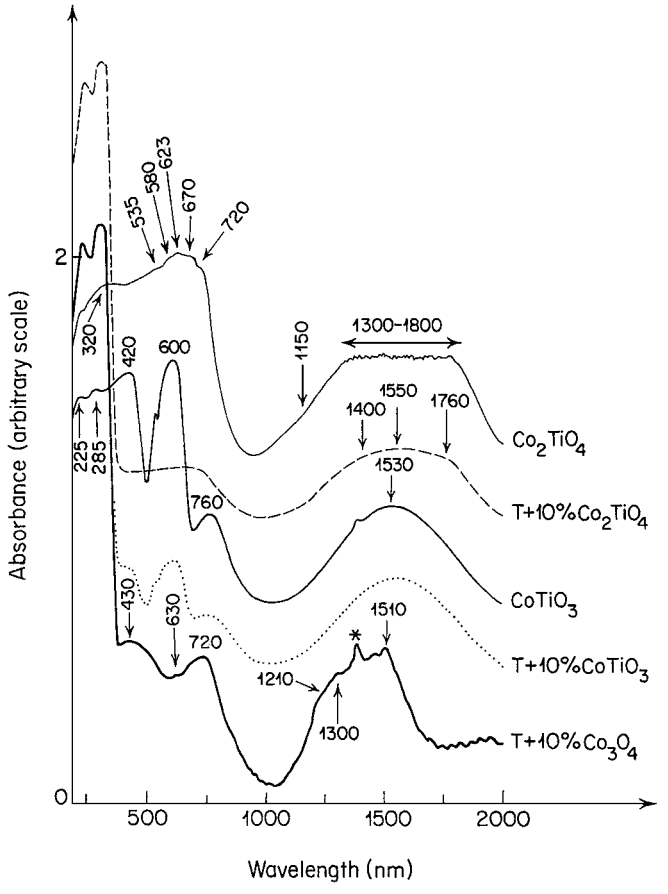

FIG. 9. DR Spectra of Co_3O_4, $CoTiO_3$,Co_2TiO_4, and of their mechanical mixtures (10% wt) in titania.

stream: (i) in the NIR, there is the appearance of a shoulder near 1750 nm (Fig. 8), also observed in Co_2TiO_4 and ascribed to the ν_2 transition of tetrahedral Co^{2+}, in agreement with the data obtained with cobalt-doped glasses (23); (ii) in the visible region, the formation of a band at 630 nm (ν_3 of tetrahedral Co^{2+}) and a shoulder around 750 nm (ν_2, octahedral Co^{2+}) well detected after 2 h are observed. A small peak appears also after 3 h at 590 nm (ν_2, tetrahedral Co^{2+}). At the end of all these transformations, the catalyst activity reaches a stationary state. These spectral modifications result from the changes of the concentration of the various cobalt species. The fresh catalyst contains mainly octahedral Co^{2+} and Co_3O_4 (cf. Fig. 2). The additional absorptions recorded "after work" are ascribed to the formation of $CoTiO_3$ and Co_2TiO_4, as suggested by Fig. 9 which shows the spectra of these reference compounds diluted in titania (see below).

In contrast, phosphorus addition to Co(7.6)/TiO_2 leads to a marked decrease of the catalysts performances in ethane ODH (Fig. 6). The extent of this effect increases with the phosphorus content and is probably due to the appearance of new cobalt species that are not active in the ODH reaction.

3.3. Catalysts Characterization after Tests

The X-ray diffraction patterns of the samples recorded after the catalytic tests (not presented) show new peaks for cobalt loading higher than 3.7 wt%. Their intensity increases with cobalt loadings. These peaks are ascribed to $CoTiO_3$ (ilmenite), Co_3O_4 (spinel), and Co_2TiO_4 (spinel) (Table 4). The presence of these phases in the catalysts is confirmed by DRS. Their spectra (Fig. 9) may be compared

TABLE 4

X-Ray Analysis of the Samples after the Catalytic Runs

Samples	Identified phases
Co(0.7)/TiO_2	TiO_2 anatase
Co(1.8)/TiO_2	TiO_2 anatase
Co(3.7)/TiO_2	TiO_2 anatase
Co(5.6)/TiO_2	TiO_2 anatase + Co_3O_4 + $CoTiO_3$
Co(7.6)/TiO_2	TiO_2 anatase + Co_3O_4 + $CoTiO_3$ + Co_2TiO_4
Co(11.5)/TiO_2	TiO_2 anatase + Co_3O_4 + $CoTiO_3$ + Co_2TiO_4
Co(15.6)/TiO_2	TiO_2 anatase + Co_3O_4 + $CoTiO_3$ + Co_2TiO_4

Note. Co_2TiO_4 : JCPDS file number 39-1410; $CoTiO_3$: JCPDS file number 77-1373.

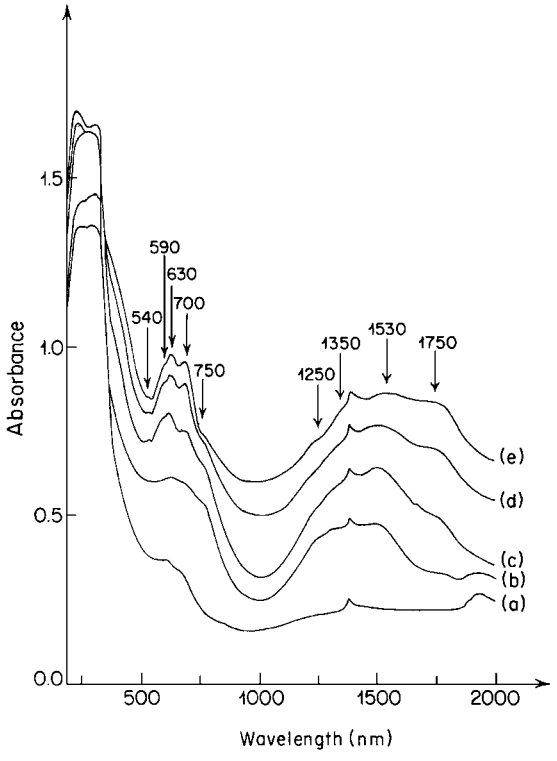

FIG. 10. DR Spectra of Co(x)/TiO_2 catalysts recorded after the catalytic tests: (a) Co(3.7), (b) Co(5.6), (c) Co(7.6), (d) Co(11.5), (e) Co(15.6).

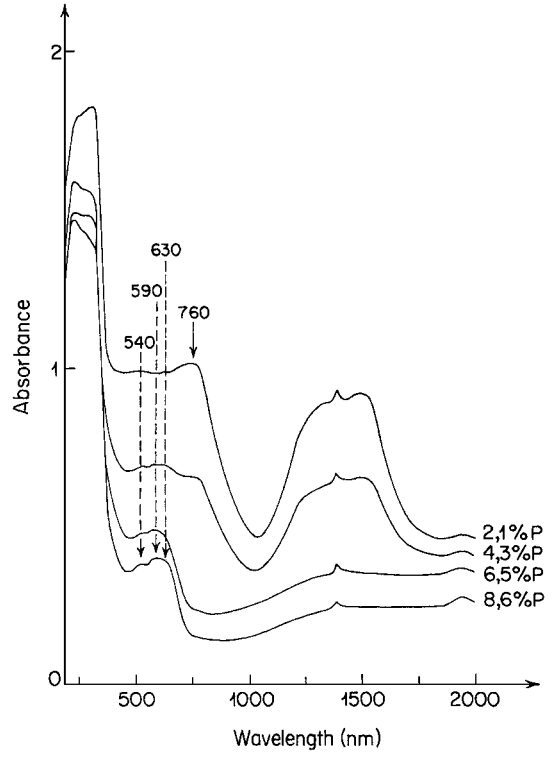

FIG. 11. Co(7.6)/TiO_2 catalyst: influence of phosphorus content on the DR Spectra recorded after the catalytic tests at 550°C.

with the spectra of Co(7.6)/TiO_2 sample recorded after the catalytic runs (Fig. 10), which are similar to those obtained at the end of the *in situ* experiments (Fig. 8, see above). Although their absorption range are partially overlapping, these compounds may be identified by specific bands:

- $CoTiO_3$ by the band at 760 nm (ν_2, octahedral Co^{2+}), also observed in Co_2SiO_4 (28) and hardly detected in Co_2TiO_4 (overlapping with ν_1 of tetrahedral Co^{2+});
- Co_2TiO_4 by the band at 1750 nm (ν_2, tetrahedral Co^{2+}), also observed in Co-doped glasses (23);
- Co_3O_4 by the bands around 700–720 nm and 420 nm (ν_1 and ν_2, octahedral Co^{3+}).

The catalytic tests performed on these compounds did not modify their diffuse reflectance spectra.

In contrast, the spectra of phosphorus-loaded samples, recorded after the catalytic runs, depend on the P content (Fig. 11, to be compared with Fig. 3). (i) For samples containing 2.1 and 4.3 wt% P, the "catalytic work" increases the intensity of the band at 750 nm and of the massif in the NIR. This may be ascribed to the formation of $CoTiO_3$. (ii) For higher P contents, no significant change is detected. This is consistent with the very low ethane conversion arising from the poisoning effects of cobalt sites by phosphorus species (cf. Section 3.1).

The Laser Raman spectra of the Co(x)/TiO_2 samples recorded after the catalytic tests and of pure $CoTiO_3$ are presented in Fig. 12. $CoTiO_3$ presents bands at 688, 450, 379 332, 263, and 233 cm^{-1} and is detected for cobalt concentration superior to 5.6 wt%. The most intense band (around 700 cm^{-1}) was also observed in isostructural compounds such as (Ni, Fe, Mg)TiO_3 and was assigned to the elongation vibration A_{1g} of the (CoO_6) octahedral units (38). In addition, weak bands assigned to Co_3O_4 are also detected. No conclusion can be drawn concerning Co_2TiO_4 which does not exhibit any Raman active band in the spectral range investigated (200–800 cm^{-1}).

Table 5 compares the XPS data before and after catalysis. At low cobalt loadings, the BE and S/M ratios do not change. However, for Co $\geq$ 7.6 wt%, they increase

TABLE 5

XPS Analysis of the Catalysts before and after Catalysis

	Before catalysis		After catalysis	
	Co $2p_{3/2}$		Co $2p_{3/2}$	
Samples	BE	S/M	BE	S/M
$Co(1.8)TiO_2$	781.1	0.43	781.4	0.44
$Co(3.7)TiO_2$	781	0.42	781.2	0.47
$Co(7.6)TiO_2$	780.2	0.27	781.1	0.45
$Co(15.6)TiO_2$	779.9	0.19	781.2	0.43
Co_2TiO_4	781	0.40	781	0.40
Co_2TiO_3	781.2	0.47	781.2	0.47

TABLE 6

Catalytic Performances of Co_3O_4, $CoTiO_3$, and Co_2TiO_4 at 550°C

Samples	Calcination temperature (°C)	S_{BET} ($m^2 \cdot g^{-1}$)	C_2H_6 Conversion (%)	C_2H_4 yield (%)	$S(C_2H_4)$ (%)	$S(CO_x)$ (%)
Co_3O_4	550	43	10.2	3.6	35	65
$(Co_3O_4 + CoTiO_3 + Co_2TiO_4)^a$	550	51	19.9	6	30	70
$CoTiO_3$	1150	9.4	21.6	3.6	16	84
$(Co_3O_4 + CoTiO_3 + Co_2TiO_4)^b$	550	49	21.4	4.6	21.5	78.5
Co_2TiO_4	1150	10	19.7	3.5	18	82
$Co(7.6)/TiO_2$	550	63.5	22.2	13.3	60	40

[a] With the ratio Co/Ti = 1.
[b] Co/Ti = 2.

significantly and approach the values recorded for Co^{2+} ions in $CoTiO_3$ and Co_2TiO_4. This suggests that the Co_3O_4 initially present in these samples has been partially reduced into $CoTiO_3$ and Co_2TiO_4.

In order to clarify their role in ethane ODH, $CoTiO_3$, Co_2TiO_4, and Co_3O_4 were tested at 550°C (Table 6). The conversion is about 20% on both $CoTiO_3$ and Co_2TiO_4 but two times less on Co_3O_4 which presents a much higher specific surface area. However, the selectivity to ethylene is two times better on Co_3O_4. For comparison, mixtures of titania and cobalt nitrate with Co/Ti ratios of 1 and 2, respectively, were prepared at 550°C. The products obtained contain the three phases (as shown by XRD analysis) and give a conversion close to that measured on pure compounds although the specific surface is four times higher. Whereas the conversions on $CoTiO_3$ and Co_2TiO_4 are close to that obtained on the best catalyst (22% on $Co(7.6)/TiO_2$), the ethylene selectivity on these compounds is much lower (16–18% instead of 60%). These results suggest that they can be correlated with the presence on the catalyst of Co^{2+} ions in octahedral sites.

The decrease of activity after "work" may be ascribed to the abatement of active surface (Table 1) arising from (i) the increase of titania crystallite size, shown by XRD, (ii) the decrease of the exposed fraction of octahedral Co^{2+} ions, arising from their aggregation into $CoTiO_3$ and Co_2TiO_4 phases. The selectivity lowering (Fig. 6) might probably be associated with the reduction of Co^{3+} ions (in Co_3O_4) into Co^{2+}-containing compounds in tetrahedral symmetry.

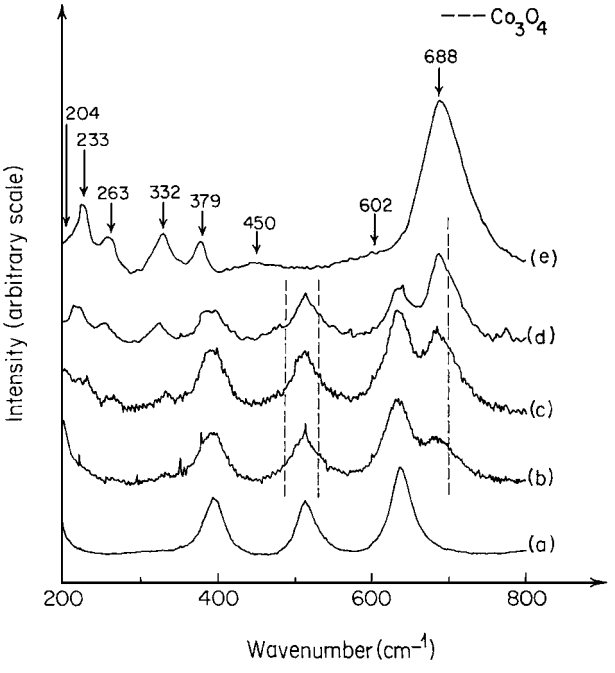

FIG. 12. Raman spectra of $Co(x)/TiO_2$ catalysts recorded after the catalytic tests: (a) Co(3.7), (b) Co(5.6), (c) Co(7.6), (d) Co(11.5): comparison with $CoTiO_3$.

4. CONCLUSIONS

Cobalt–titania (anatase) catalysts prepared by impregnation and calcination at 550°C contain dispersed octahedral Co^{2+} ions and Co_3O_4. *In situ* UV–visible DR examination during and after the catalytic tests showed that these entities are transformed (partially at least) into $CoTiO_3$ and Co_2TiO_4 phases. These three compounds were identified on the catalysts by XRD, XPS, and LRS spectroscopy.

The activity of cobalt–titania (anatase) catalysts in ethane ODH is maximum for a Co content of about 7.6 wt%. The ethylene yield reaches 13.3% at 550°C. Addition of phosphorus leads to a marked activity decrease, ascribed to the formation of cobalt–phosphorus compounds not active in the reaction.

The results also suggest that the activity can mainly be correlated with the presence of Co^{2+} species in octahedral symmetry.

ACKNOWLEDGMENTS

The authors are indebted to the French Ministère des Affaires Etrangères for financial support (Action Intégrée 183/MA/99). The ITODYS laboratory (Université Paris 7-Denis Diderot) is gratefully

acknowledged for XPS and LRS analyses. The help of M. Potvin (Laboratoire de Réactivité de Surface, Université Pierre et Marie Curie) in XRD measurements was also greatly appreciated.

REFERENCES

1. Kung, H. H., *Adv. Catal.* **40**, 1 (1994).
2. Thorsteinson, E. M., Wilson, T. P., Young, F. G., and Kassai, P. O. H., *J. Catal.* **52**, 116 (1978).
3. Murakami, V., Otsuka, K., Wada, Y., and Morikawa, A., *Bull. Soc. Jpn.* **63**(2), 340 (1990).
4. Eastman, A. D., Guillory, J. P., Cook, C. F., and Kimble, J. B., U.S. Patent 4,497,971 (1985).
5. Loukah, M., Coudurier, G., Védrine, J. C., and Ziyad, *M., Micropor. Mater.* **4**, 345 (1995).
6. (a) El-Idrissi, J., Kacimi, M., Loukah, M., and Ziyad, M., *J. Chim. Phys.* **94**, 1984 (1997); (b) El-Idrissi, J., Kacimi, M., Bozon-Verduraz, F., and Ziyad, M., *Catal. Lett.* **56**, 221 (1998).
7. (a) Bañares, M. A., Martínez-Huerta, M. V., Gao, X., Fierro, J. L. G., and Wachs, I. E., *Catal. Today* **61**, 295 (2000); (b) Ciambelli, P., Galli, P., Lisi, L., Massucci, M. A., Patrono, P., Pirone, R., Ruoppolo, G., and Russo, G., *Catal. Today* **302**, 133 (2000).
8. (a) Li, J., and Coville, N. J., *Appl. Catal. A.* **181**, 201 (1999); (b) Anderson, R. B., "The Fischer–Tropsh Synthesis." Academic Press, New York, 1984; (c) Schulz, H., Schon, M., and Rahman, N. M., Cerveny, L., (Editor), *in* "Catalytic Hydrogenation" (Le. Cerveny, Ed.), Stud. Surf. Sci. Catal., Vol. 27, p. 201. Elsevier, Amsterdam, 1986.
9. Ho, S. W., Cruz, J. M., Houalla, M., and Hercules, D. M., *J. Catal.* **135**, 173 (1992).
10. (a) Koerts, T., and Van Santen, R. A., *J. Chem. Soc. Chem. Comm.* 1281 (1991); (b) Pareja, P., Amariglio, A., Belgued, M., and Amariglio, H., *Catal. Today* **21**, 423 (1994).
11. Voorhoeve, R. J. H., *in* "Advances Materials in Catalysis" (J. Burton and R. L. Garten, Eds.). Academic Press, New York, 1977.
12. Pedersen, L. A., and Libby, W. F., *Science* **176**, 1355 (1972).
13. Centi, G., and Trifiro, F., "New Developments in Selective Oxidation." Elsevier, Amsterdam, 1990.
14. Heuel, R. C., and Bartholomew, C. H., *J. Catal.* **85**, 78 (1984).
15. Che, M., and Bozon-Verduraz, F., *in* "Handbook of Heterogeneous Catalysis," Vol. 2, p. 641, 1997.
16. Weckhuysen, B. M., and Schoonheydt, R. A., *Catal. Today* **49**, 441 (1999).
17. Scofield, J. H., *J. Electron Spectr. Relat. Phenom.* **8**, 129 (1976).
18. Legrouri, A., Ramdhane, S. S., Lenzi, J., Lenzi, M., and Bonel, G., *J. Mater. Sci.* **31**, 2469 (1996).
19. Noronha, F. B., Perez, C. A., Schmal, M., and Fréty, R., *Phys. Chem. Chem. Phys.* **1**, 2861 (1999).
20. Wood, D. L., and Remeika, J. P., *J. Chem. Phys.* **46**, 3595 (1967).
21. Jacono, M. L., and Cimino, A., *Gazz. Chim. Ital.* **103**, 1281 (1973).
22. Okamoto, Y., Nagata, K., Adachi, T., Imanaka, T., Inamura, K., and Takyu, T., *J. Phys. Chem.* **95**, 310 (1991).
23. Bizi, M., Ph.D. thesis, University of Rouen, France, 1989.
24. Pappalardo, R., Wood, D. L., and Linares, R. C., *J. Chem. Phys.* **35**, 2041 (1961).
25. Low, W., *Phys. Rev.* **109**, 247 (1958).
26. Verberckmoes, A., Weckhuysen, B. M., and Schoonheydt, R. A., *Micropor. Mesopor. Mater.* **22**, 165 (1998).
27. Goodgame M., and Cotton, F. A., *J. Phys. Chem.* **85**, 791 (1961).
28. Blasse, G., *Struct. Bonding* **76**, 153 (1991).
29. Lever, A. B. P., "Inorganic Electronic Spectroscopy," p. 480. Elsevier, Amsterdam, 1984.
30. Kraushaar-Czarnetzki, B., Hoogervorst, W. G. M., Andréa, R. R., Emeis, C. A., and Stork, W. H. J., *J. Chem. Soc. Faraday Trans.* **87**(6), 891 (1991).
31. Stranick, M. A., Houalla, M., and Hercules, D. M., *J. Catal.* **106**, 362 (1987).
32. Jezlorowski, H., Knozinger, H., Grange, P., and Gajardo, P., *J. Phys. Chem.* **84**, 1825 (1980).
33. De Boer, D. A., Haas, C., and Sawatzky, G. A., *Phys. Rev. B* **29**, 4401 (1984).
34. Veal, B. W., and Paulikas, A. P., *Phys. Rev. B* **31**, 5399 (1985).
35. Sexton, B., Hughes, A., and Turney, T. W., *J. Catal.* **97**, 390 (1986).
36. Bonnelle, J. P., Grimblot, J., and D'huysser, A., *J. Electron. Spectrosc.* **6**, 71 (1975).
37. Frydman, A., Castner, D. G., Schmal, M., and Campbell, C. T., *J. Catal.* **152**, 164 (1995).
38. Baraton, M. I., Busca, G., Prieto, M. C., Ricchiardi G., and Escribano, V. S., *J. Solid State Chem.* **112**, 9 (1994).